Supporting information file for publication

Optimization of electromagnetic hot spots in surface-enhanced Raman scattering substrates for an ultrasensitive drug assay of emergency department patients' plasma

Thakshila Liyanage,[1] Adrianna N. Masterson,[1] Sumon Hati,[1] Greta Ren,[1] Nicholas E. Manicke,[1] Daniel E. Rusyniak,[2] and Rajesh Sardar*,[1]

[1]Department Chemistry and Chemical Biology, Indiana University-Purdue University Indianapolis, Indianapolis, Indiana, 46202, United States

[2]Department of Emergency Medicine, Indiana University School of Medicine, 720 Eskenazi Avenue, Indianapolis, Indiana, 46202, United States

S1. Synthesis of Polyethylene glycol thiol, n = 60 (PEG60-SH). Accordingly 25 g (12.5 mmol) of polyethylene glycol and 50 mL of tetrahydrofuran (THF) was mixed in round bottom flask kept in ice under nitrogen for 10 min and then 0.75 g (18.6 mmol) of sodium hydroxide was dissolved in 50 mL of water and was added to the reaction mixture at 0 ^{O}C, and allowedto stir for another 15 min under nitrogen. Then 7.15 g (37.5 mmol) of 4-Toluenesulfonyl chloride (TsCl) was mixed in 50 mL THF and added dropwise to the above reaction mixture at 0 ^{o}C over 30 min. The reaction was allowed to warm to room temperature and was stirred for at least 48 h under nitrogen. Then THF was evaporated and the reaction mixture was washed thoroughly four to five times with hexane using a separating funnel. Finally, phase transition was carried out using dichloromethane (DCM), and the DCM solution containing PEG60-OTsCl was dried over Na_2SO_4. A white solid of PEG60-OTsCl was obtained after evaporating the DCM. NMR analysis was conducted to confirm the product. ^{1}H NMR (500 MHz, $CDCl_3$) δ ppm: 2.43 (s); 3.36 (s); 3.52-3.68 (m); 4.13-4.15 (t); 7.32-7.34 (d); 7.77-7.79 (d).

15.4 g (7.2 mmol) of PEG60-OTsCl was mixed with 0.60 g (8.6 mmol) of thiourea in 100 mL ethanol and then refluxed overnight. Next, 34.4 mg (8.6 mmol) of NaOH dissolved in 5 mL nanopure water was added and refluxing continued for another 3 h. The reaction mixture was allowed to cool to room temperature and the ethanol was evaporated, followed by the addition of 100 mL of water. The aqueous solution was acidified using concentrated HCl. The reaction mixture was thoroughly washed using ethyl acetate at least four times and finally phase transition was carried out with DCM. The DCM solution was dried using Na_2SO_4. Finally, DCM was evaporated, and a white solid of PEG60-SH was collected. NMR was utilized confirm the product. ^{1}H NMR (500 MHz, $CDCl_3$) δ ppm: 1.16-1.58 (t); 2.64-2.68 (m); 3.34 (s); 3.48-3.65 (m).

S2. Functionalization of Glass Coverslips and Silicon Wafers. Glass coverslips were silanized using our previously published method. Glass coverslips were immersed in a 10% (v/v) aqueous RBS 35 detergent solution at 90 ^{0}C and sonicated for 10 min. After that,

coverslips were cleaned with copious amount of nanopure water to remove all soap and then incubated in a solution containing concentrated HCl and methanol (1:1 v/v). After 30 min, coverslips were washed several times with nanopure water and transferred to a vacuum oven at 60 ^{0}C overnight. Next day, the dried coverslips were incubated in an ethanolic solution of 15% APTES for 30 min, followed by sonication in fresh ethanol for 10 min. The washing step was repeated four additional times and during each time, fresh ethanol was used. After the last wash, coverslips were placed in a vacuum oven at 120 ^{0}C for 3 h prior to use. The prepared APTES functionalized coverslips were then stored at 4 ^{0}C. To prepare APTES, PHTMS-, and OCTMS-functionalized silicon wafers, a similar procedure was performed. Freshly cut silicon wafers were introduced to piranha cleaning solution for 30 min, rinsed with a copious amount of water, sonicated in water for 10 min, and then placed in a vacuum oven at 60 ^{0}C overnight. The following day procedure was identical to that for the glass coverslips.

S3. SERS Measurements. SERS measurements were conducted using a Foster-FORAM 785 HP Raman system with a 785 nm diode laser excitation source with 20 mW of power and 5-μm spot size. Automatic baseline correction was performed using OMNIC software before acquired spectra were plotted.

S4. UV-Vis-NIR Measurements. A Varian Cary 50 Scan UV-visible spectrophotometer was used to collect absorption and extinction spectra in the range of 300-1100 nm. For the absorption spectra of Au TNP solutions, 0.3 mL of reaction mixture was diluted to a final volume of 2.0 mL with acetonitrile in a 1 cm quartz cuvette. Acetonitrile was used as a background in each run before collecting absorbance spectra. Extinction spectra of PEG60-S-functionalized Au TNPs as a nanoplasmonic superlattice substrate were collected using a Perkin Elmer Lambda 19 UV-Vis-NIR spectrometer. APTES-/PHTMS-/OCTMS-functionalized glass coverslips were used as a background.

S5. Scanning Electron (SEM) and Transmission Electron (TEM) Microscopy Analyses. Nanoplasmonic superlattice substrates were imaged using a JEOL 7800F instrument. TEM analysis was conducted using a Tecnai-12 instrument at 100 kV operating voltage. Colloidal acetonitrile solution of Au TNPs was drop-casted onto a Cu-carbon grid and the solvent was allowed to dry a room temperature before imaging.

S6. Contact Angle Measurements. We used Ramé-Hart Contact Angle Goniometer to measure the contact angles.

S7. Limit of Detection (LOD) Calculations. Limit of detection (LOD) was calculated using previously reported complex mathematical equation (Eq.1). Accordingly, 1.0 millimolar (mM) stock solution of drug in plasma was prepared and then various dilution series with 10-fold concentration changes were created until a concentration of 100 picomolar (pM) was reached. For the blank signals, a SERS spectrum of PEG_{60}-SH functionalized coverslips were obtained.

$$LOD_B = \bar{Y}_b + t_\alpha^{n-1} s_b^{n-1} \sqrt{\frac{1+1}{n}} \quad \textbf{(1)}$$

$$\bar{Y}_b = Average\ blank\ signal\ value$$

$$t_\alpha^{n-1} = critical\ value\ of\ the\ distribtion$$

$$s_b^{n-1} = standered\ devaition$$

$$\sqrt{\frac{1+1}{n}} = Replacement\ of\ the\ true\ mean\ by\ \bar{Y}_b, n = 3\ number\ of\ blank\ spectrum$$

S8. Time-dependent density functional theory (TDDFT) Calculations. TDDFT calculations were performed to determine Raman vibrational frequencies of the drug molecules. Calculations involved geometry optimization and calculations using Gaussian16 with the B3LYP hybrid exchange correlation functional and 6-311+G** basis set[1] for free drug molecules and drug molecules attached to glycol moiety. Calculations were also performed for drug molecules attaching to gold (Au) atom using the BP86 exchange-correlation functional and the LanL2DZ effective core potential basis set.[2] Gaussview 6.0.16 was used to visualize the optimized geometry and assign the vibrational modes.[3]

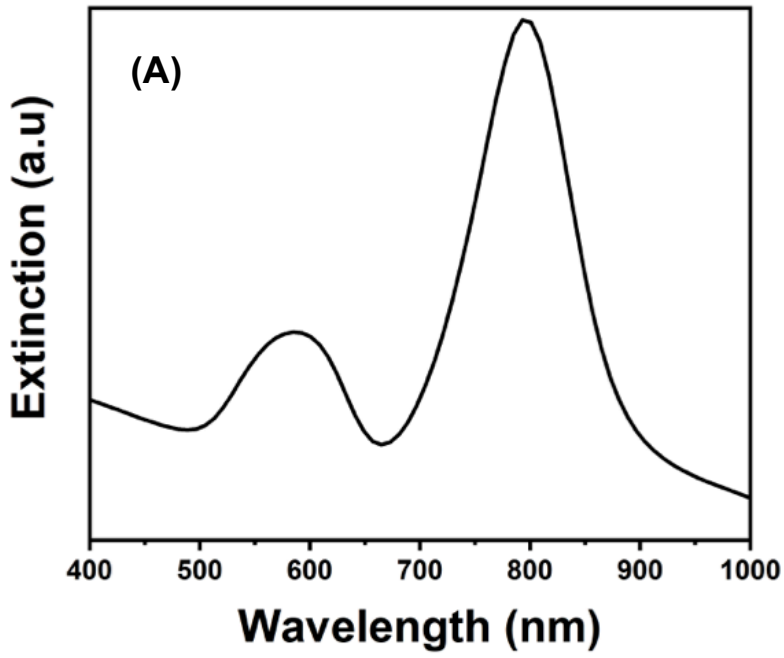

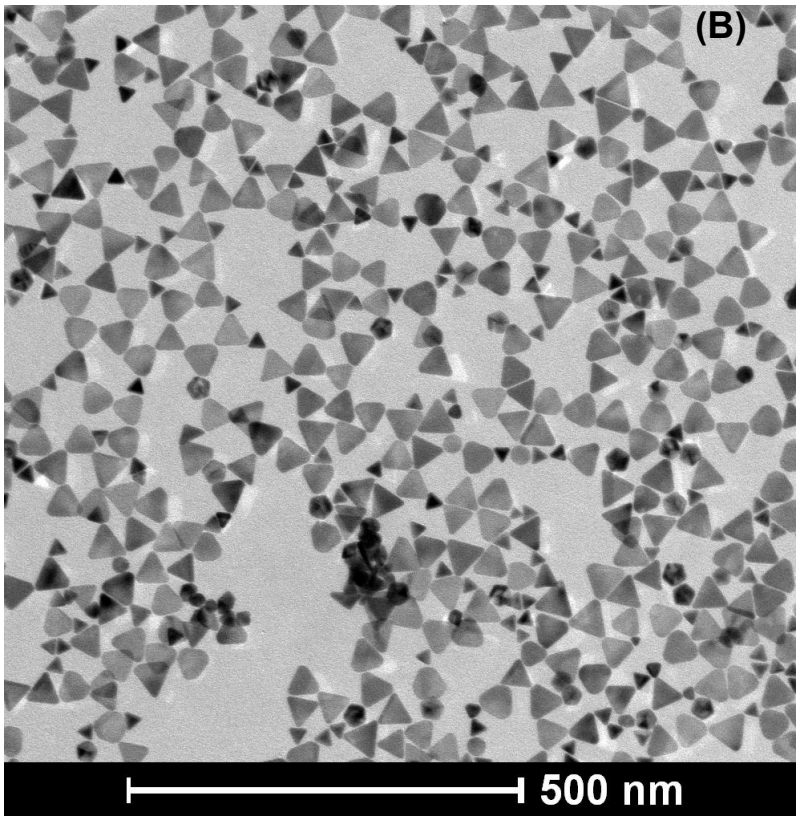

Fig. S1. (A) A representative UV-vis extinction spectrum of freshly synthesized TEA-passivated Au TNPs, which display an LSPR dipole peak (λ_{LSPR}) at 800 nm in acetonitrile. (B) A representative transmission electron microscopy image of Au TNPs.

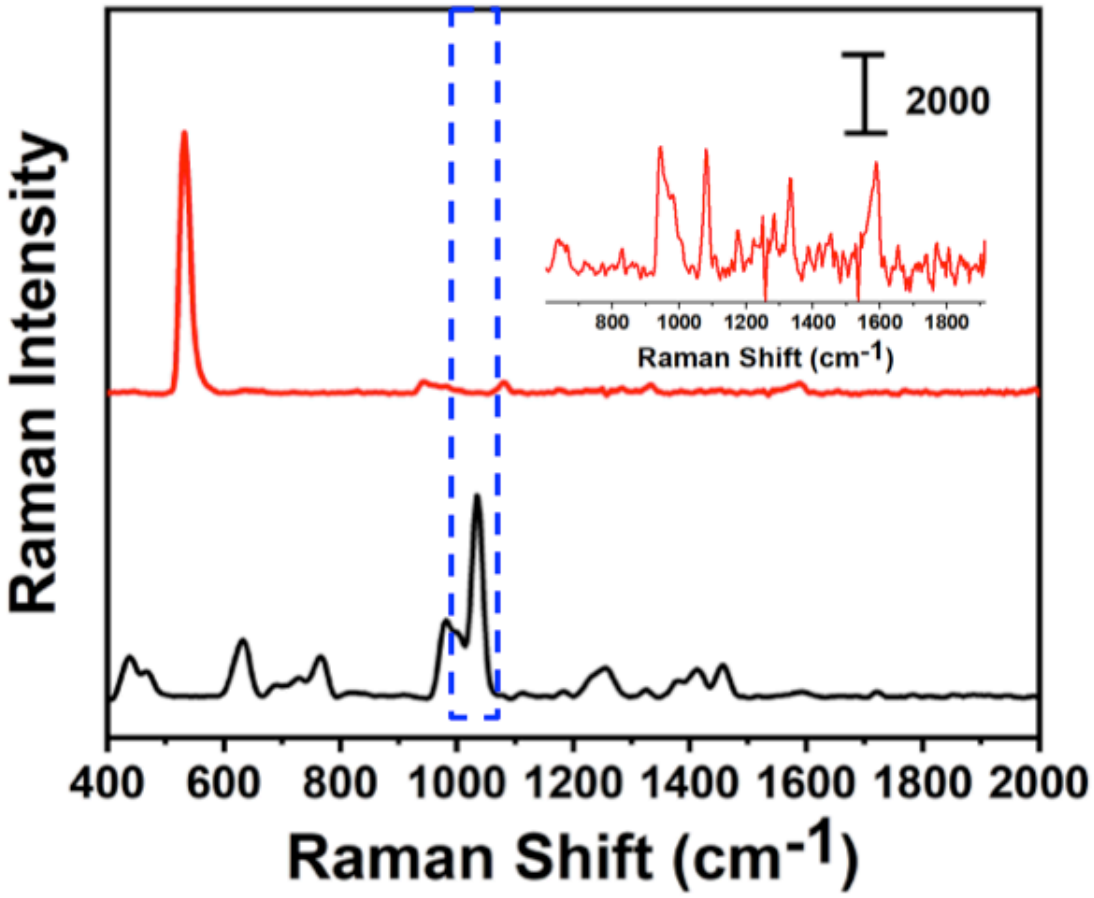

Fig. S2. (Bottom) The SERS spectrum of TEA-passivated Au TNPs. The Raman stretch at 1035 cm^{-1} is assigned to the C-N stretch of TEA used for the synthesis of the Au TNPs. **(Top)** The SERS spectrum collected after 24 h ligand exchange with 1.0 mM of PEG60-SH. The complete disappearance of C-N stretch (1035 cm^{-1}, blue dotted box) confirms the successful replacement of TEA, and the formation of PEG60-S-functionalized Au TNPs. The inset shows an expanded version of the top spectrum showing peaks at 645, 944, 1083, 1100 and 1177, and 1334 cm^{-1} for aliphatic C-S stretch, C-H bending, COC symmetric stretch, and CH_2 stretch, respectively.[4] The scale bar is for the overall spectra and not for the inset.

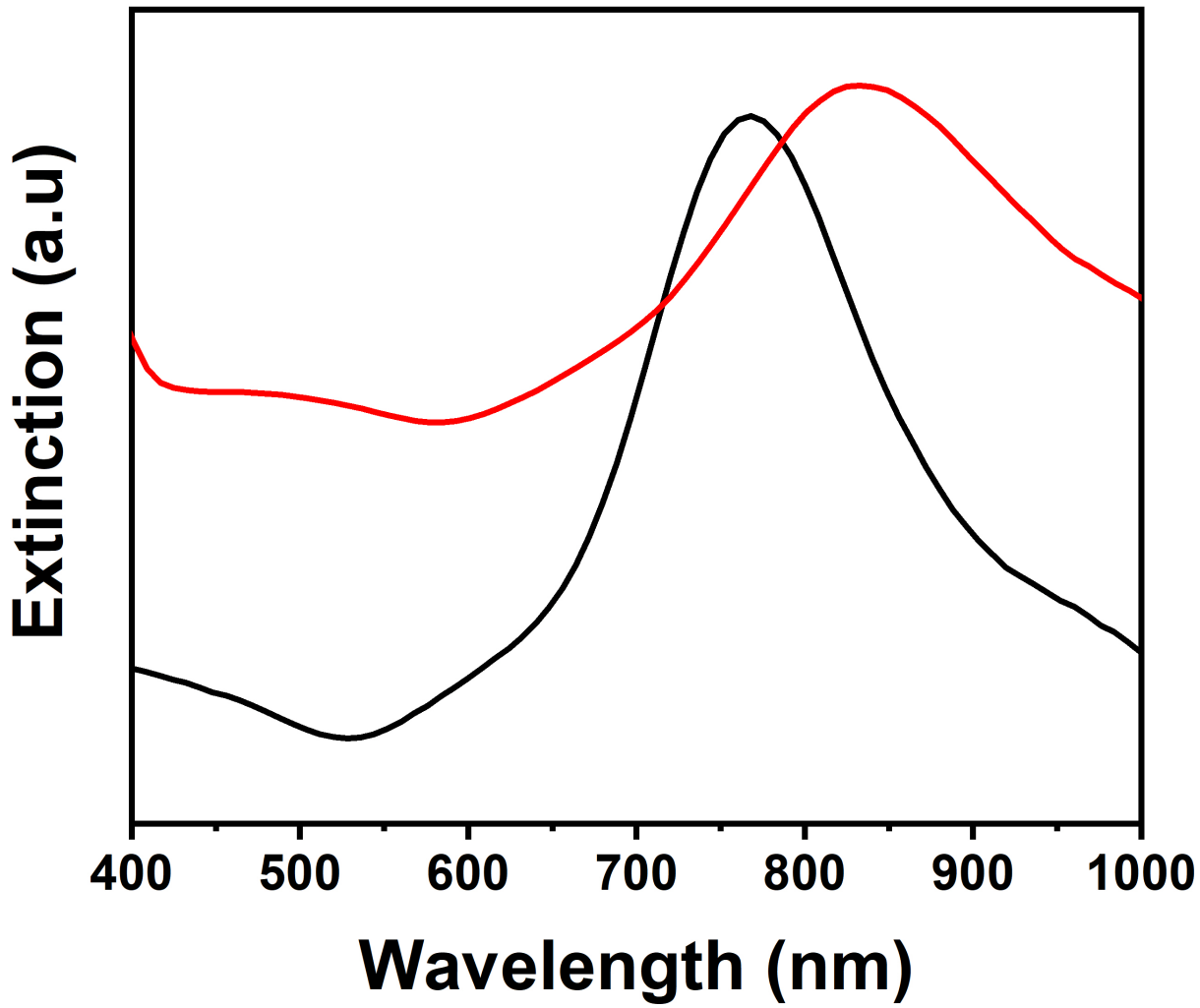

Fig. S3. An UV-vis extinction spectrum of TEA-passivated Au TNPs attached onto an APTES-modified glass support. The LSPR dipole peak is at 775 nm (black). Ligand exchange with 1.0 mM PEG60-SH produces a red shift in the LSPR dipole peak and is appeared at 835 nm. All extinction spectra were collected in air.

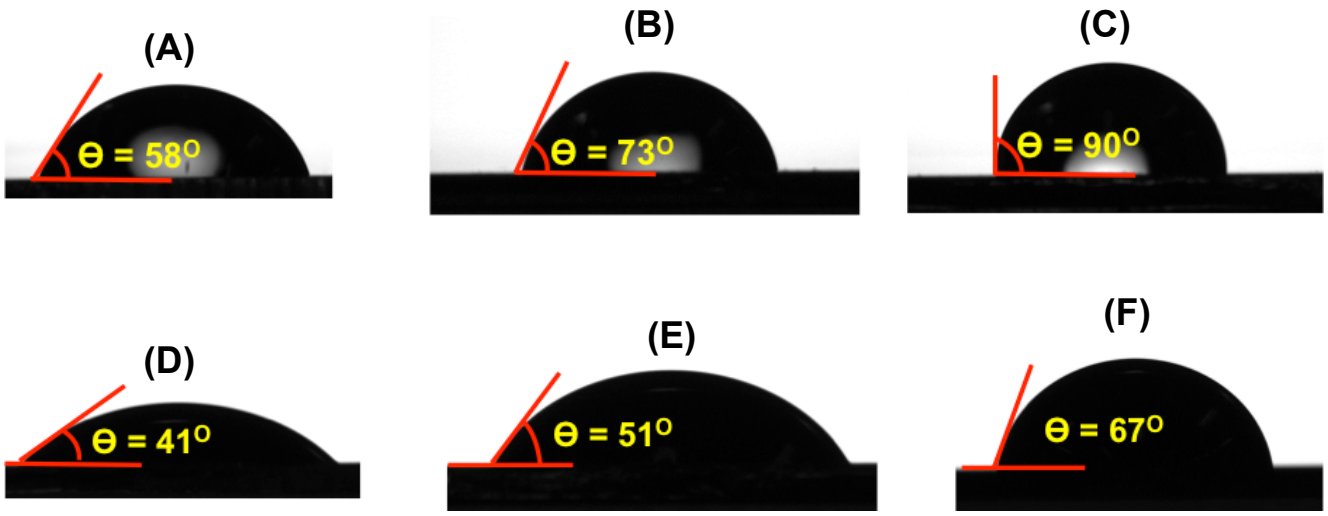

Fig. S4. Contact angle images for the water droplet on (A) APTES-, (B) PHTMS-, and (C) OCTMS-modified glass supports. Contact angle images for an aqueous colloidal solution of PEG60-S-functionalized Au TNPs droplet on (D) APTES-, (E) PHTMS-, and (F) OCTMS-modified Si wafer.

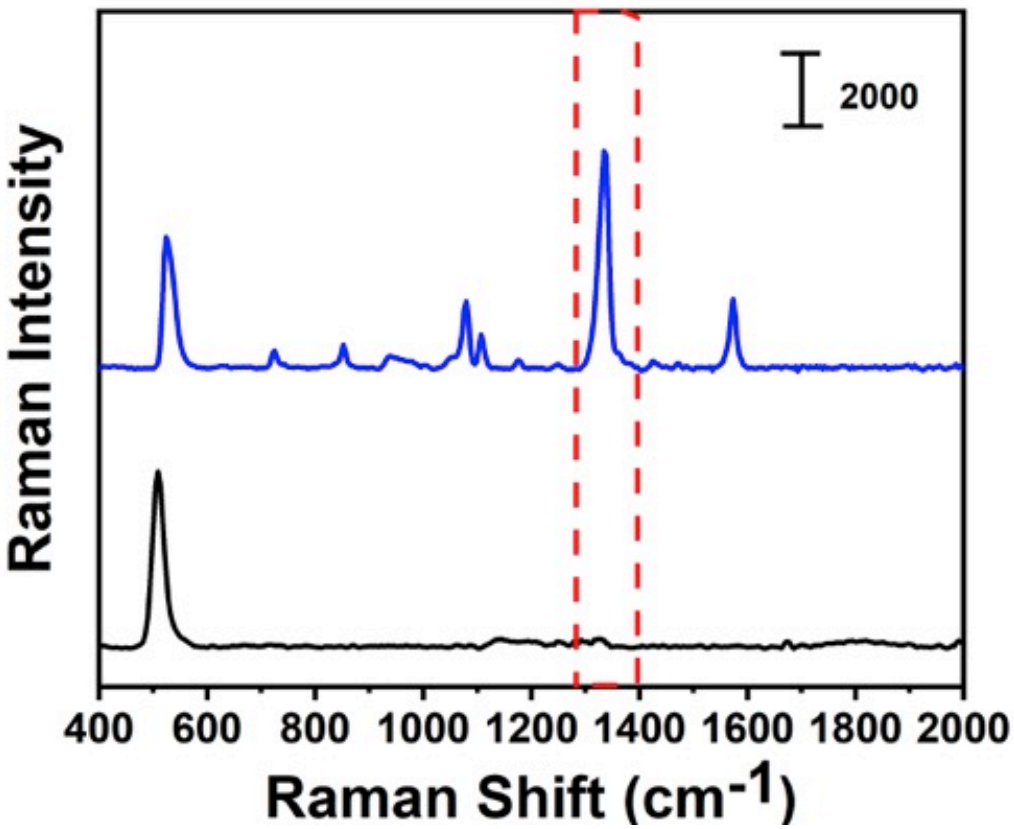

Fig. S5. Black curve represents the normal Raman spectrum of 1.0 mM fentanyl on silicon wafer. Blue curve represents the SERS spectrum of 100 pM fentanyl Substrate-3. For the AEF calculation we used C-N stretch of fentanyl at 1334 cm^{-1} as shown in the dotted red box.

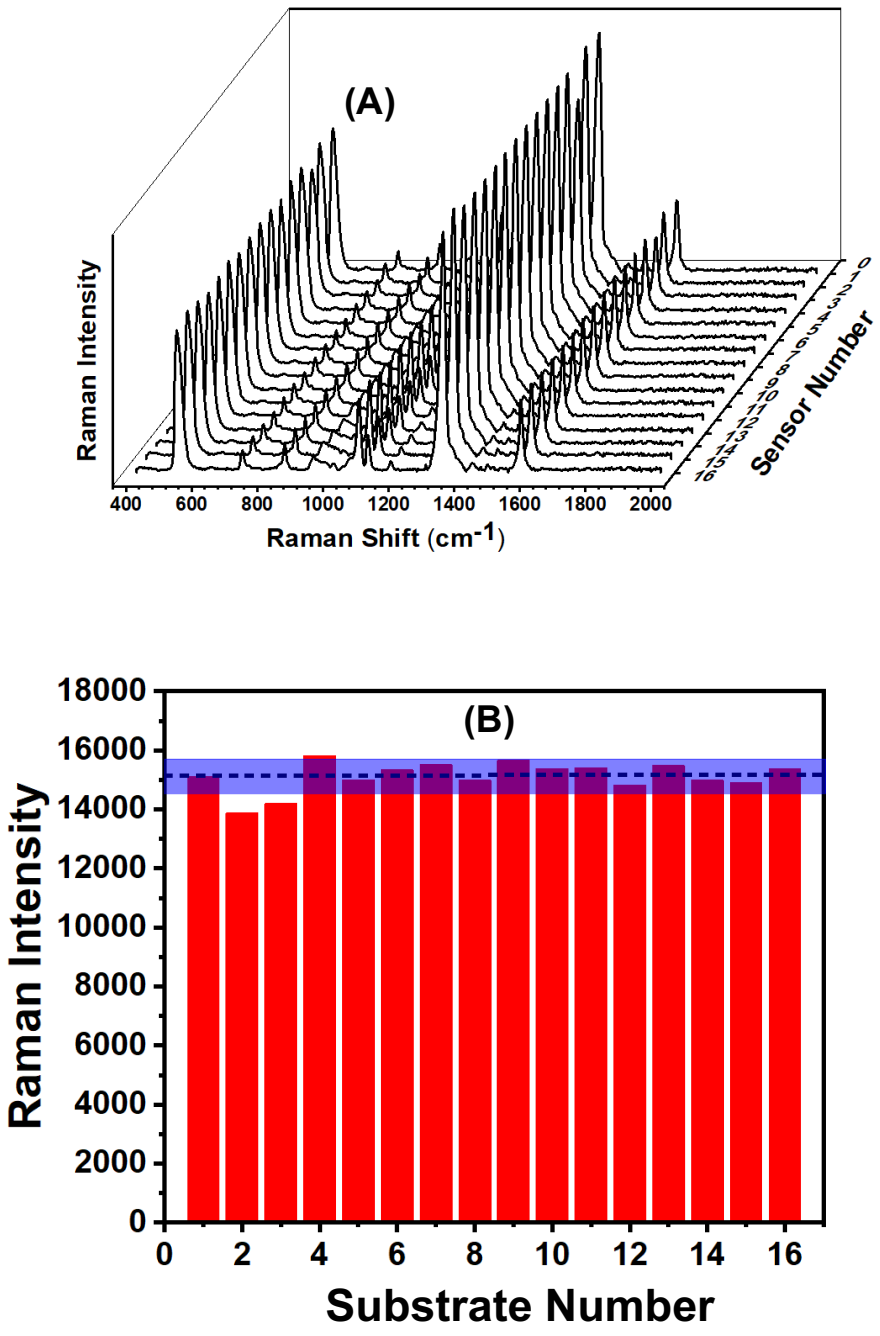

Fig. S6. (A) The reproducibility of our developed nanoplasmonic superlattice for SERS-based drug analysis. SERS spectra of 1.0 μM fentanyl were collected from 16 different substrates. **(B)** The bar graph shows relative standard deviation of 3.8% amongst 16 superlattices.

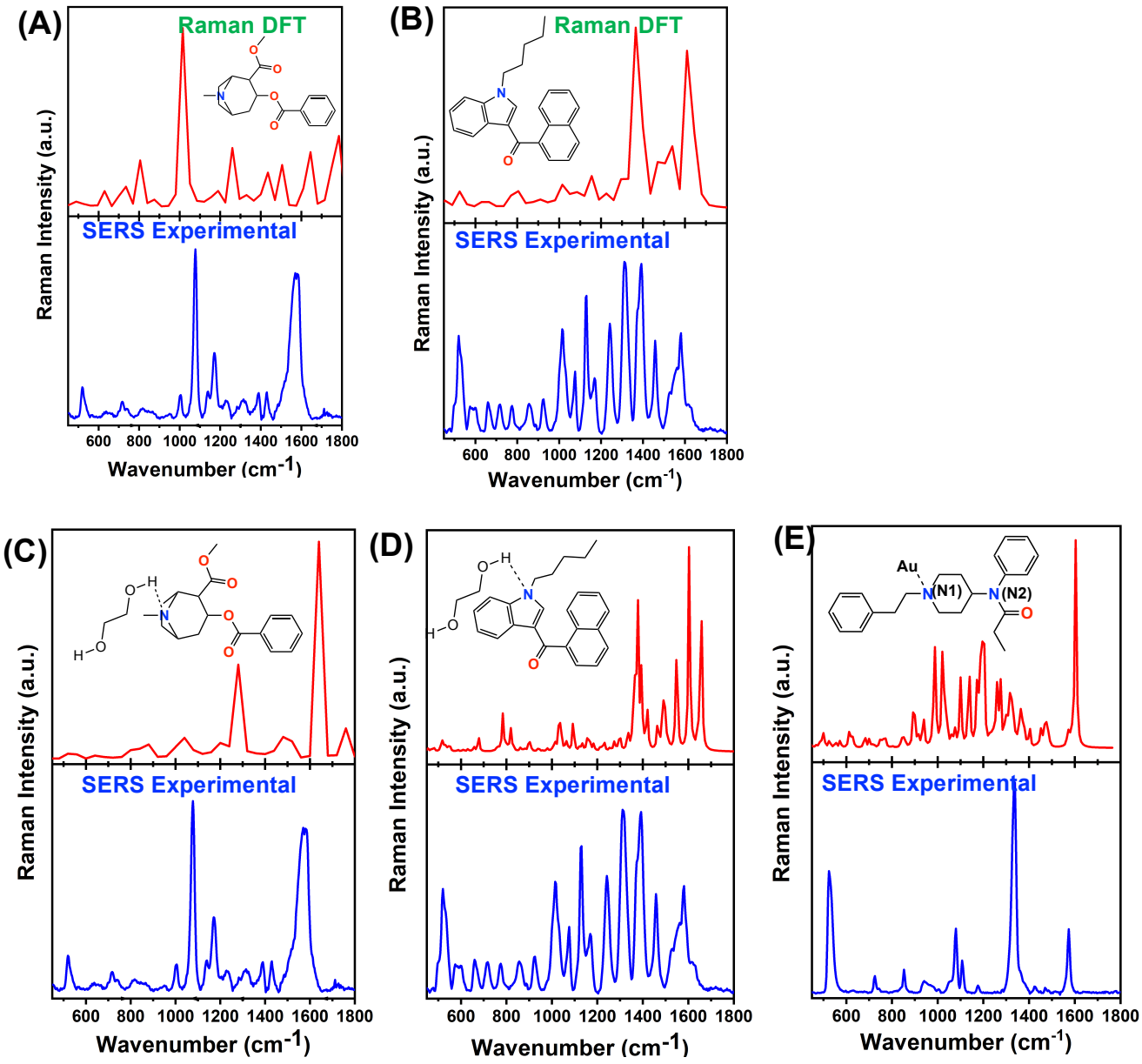

Fig. S7. DFT-calculated Raman spectra of cocaine (A) and JWH-018 (B). Experimental SERS spectra (blue curve) and DFT-calculated Raman spectra (red curve) of (C) cocaine, (D) JWH-018, and (E) fentanyl in which their nitrogen atom formed hydrogen bonding with ethylene glycol.

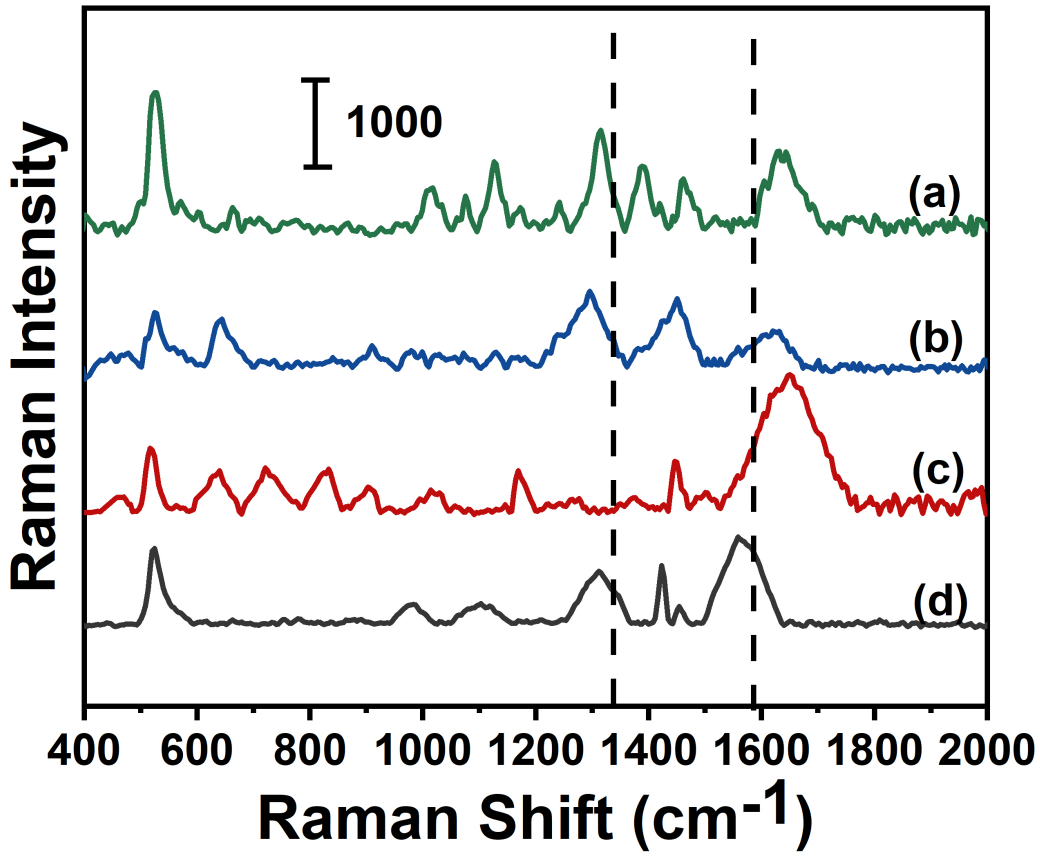

Fig. S8. SERS spectra of four-patient sample collected using Substrate-3. Black dashed lines represent position of C-N stretch at1334 cm^{-1} of fentanyl and the C=C stretch at 1586 cm^{-1} for cocaine. No real peak associated with these two drugs are identified. Drug compositions identified in these samples from paper spray ionization-mass spectrometry are: (a)-JWH-149, (b)-U47700 and oxazepam, (c)-ketamin, methadone, and midazolam, and (d)-methamphetamine and U47700.

Table S1. Summary of SERS-substrates used for drug detection in human bodily fluids found in the literature.

SERS Material	Type of Drug	Sensitivity	Sample	Reference
Gold and silver sol-gels	Cocaine	25 ppb	Saliva	4
gold- and silver- doped sol-gels immobilized in glass capillaries	Cocaine	50 ppb	Saliva	5
paper-based substrate made of lab-grade filter paper immersed in a colloidal suspension of silver nanoparticles	Fentanyl and as an adulterant in heroin	100 ppb	Purchased Chemical	6
Gold nanoparticle co-aggregation in a wet system	JWH-016, JWH-018, JWH-019, JWH-201, JWH-250, JWH-302	Not Provided	Herbal Highs Plant samples	7
Field-guided assembly of silver Nano colloids	Cocaine	Not Provided	Purchased Chemical	8
Silver nanoparticles printed on cellulose filter paper	Cocaine	15 ng	Purchased Chemical	9
Colloidal Gold Nanoparticles	JWH-018	31 ppb	Oral fluid	10
Nanoplasmonic superlattice substrate	Fentanyl	130 ppq	Human plasma	This work
Nanoplasmonic superlattice substrates	Cocaine	32 ppq	Human plasma	This work
Nanoplasmonic superlattice substrates	JWH-018	119 ppq	Human plasma	This work

Table S2. Density Functional theory-based Raman stretches of fentanyl, cocaine, and JWH-018. All the vibrational modes are assigned as reported in the literature.[10-12]

Vibrational Description	Only Fentanyl		Fentanyl-Glycol		Fentanyl-Au		Experimental
	Mode	DFT/cm^{-1}	Mode	DFT/cm^{-1}	Mode	DFT/cm^{-1}	SERS/cm^{-1}
ν (C═C)$_{B1}$	124	1,642	172	1,642	127	1,580	1,573
δ (CH$_2$)$_{pip}$	118	1,506	161	1,498	121	1,476	1,469
δ (H-C-N2)	103	1,390	142	1,399	107	1,372	1,338
ν (N1-C-C-C)$_{B1}$; γ_t (CH$_2$)$_\beta$	85	1,222	119	1,219	82	1,140	1,106
δ (CH)$_{B1,B2}$	76	1,124	106	1,102	76	1,068	1,079
ν (C═C)$_{B1,B2}$; δ (CH)$_{B1,B2}$	70	1,052	96	1,048	71	1,004	1,002
δ (C═C)$_{B2}$; ν (C$_\varepsilon$-C$_1$-C$_2$)	65	1,017	90	1,021	64	972	962
δ_r (CH$_2$)$_{pip}$; ν (C$_\varepsilon$-C$_1$-C$_2$)	57	966	83	976	59	916	937
ν (C$_{B1}$-C$_\alpha$-C$_\beta$-N$_1$); β (ring)$_{B1}$	45	778	64	751	52	820	852
γ_t (CH$_3$); δ_r (CH$_2$)$_{pip}$; δ (C$_\varepsilon$-C$_1$-C$_2$)	42	754	63	724	46	724	725
δ (ring)$_{B1,B2}$; δ_r (CH$_2$)$_{alkyl}$; δ_r (CH$_3$)	37	636	57	634	42	628	628

ν = stretching, δ = in plane deformation (*sc* = scissoring, *r* = rocking), γ = out of plane deformation (w = wagging, t = twisting), β = breathing.

Vibrational Descriptions	Cocaine-Au		Experimental
	Mode	DFT/cm^{-1}	SERS/cm^{-1}
υ (C=O, benzoate ester)	104	1,604	1,574
δ (benzene ring)	90	1,380	1,390
ω (CH, piperidine ring) + ω_s(CH$_2$, piperidine ring)	88	1,356	1,315
ν_{as} (HC−C−O) + δ (benzene ring) + ω (CH$_2$-CH, piperidine/pyrollidine ring)	79	1,236	1,228
ν (C−O, piperidine ester) + β_{as} (C−H$_3$, piperidine ester) + γ (piperidine/pyrollidine ring) + ω (C−H, piperidine ester)	68	1,180	1,170
δ (benzene ring)	55	988	1,077
ν_s (H$_2$C−CH−CH, piperidine ring) + ν_{as} (H$_2$C−CH$_2$−CH$_2$, pyrollidine ring)	48	876	1,000
γ (piperidine/pyrollidine ring)	44	804	817
γ (benzene ring)	41	756	717
δ (benzene ring)	33	620	637

υ = stretching; δ = in-plane distortion; γ = out-of-plane distortion; ω = wagging; τ = torsion; β = breathing; s = symmetric; as = antisymmetric

Vibrational Descriptions	JWH-018-Au		Experimental
	Mode	DFT/cm^{-1}	SERS/cm^{-1}
v (C=O)	120	1,604	1,581
δ_{sc} (CH_2); δ_{sc} (CH_3); δ_{sc} (CH_2) I2; δ_{sc} (CH) Nph	116	1,492	1,459
δ_r (CH) Nph	104	1,420	1,392
v (C=C) Nph	100	1,388	1,312
γ_t (CH_2); δ_{sc} (CH) I2, N2	91	1,276	1,242
δ_{sc} (HC-CH) I2, N1	83	1,188	1,168
δ_{sc} (HC-CH) Nph	78	1,140	1,127
δ_{sc} (HC-C-CH) N1	74	1,060	1,076
β (ring) I2; v (C-C) tail	69	1,012	1,014
v (C-CH_3); δ (ring) I2, Nph	60	908	922
δ_r (CH_2); δ_r (CH_3); γ_w (CH)-N-CH	52	796	856
β (ring) Ind; γ_w (CH) Nph	49	764	775
δ (ring) Nph	41	668	713
δ (ring) I1, Nph	40	644	659
δ (ring) Ind, Nph	33	508	580
γ_w (CH) Nph; δ (ring) Ind	31	468	497

ν = stretching, δ = in plane deformation (*sc* = scissoring, *r* = rocking), γ = out of plane deformation (w = wagging, t = twisting), β = breathing. Nph = Naphthalene; Ind = Indole; N1 and N2 refer to the two rings in naphthalene. I1 and I2 refer to the two rings in indole.

Table S3. SERS-based concentration determination in six drug overdose/abuse patient plasma from the ED. Column 2 provides specific identity of drugs determined from the paper spray ionization-mass spectrometry analysis.

Sample Number	Analyte Type	Concentration of cocaine in 10% diluted plasma sample (pg/μL)	Concentration of fentanyl in 10% diluted plasma sample (pg/μL)
(a)	Cocaine	1.47	
(b)	Cocaine	0.23	
(c)	Fentanyl or acryl fentanyl, cocaine, furanyl fentanyl	0.11	0.13
(d)	AB-PINACA, Furanyl Fentanyl, Methamphetamine		0.40
(e)	Acrylfentanyl or Fentanyl, Codeine		0.36
(f)	Acryl fentanyl or fentanyl, furanyl fentanyl		0.22

S9. References

1. M. J. T. Frisch, G. W.; Schlegel, H. B.; Scuseria, G. E.; Robb, M. A.; Cheeseman, J. R.; Scalmani, G.; Barone, V.; Petersson, G. A.; Nakatsuji, H.; Li, X.; Caricato, M.; Marenich, A. V.; Bloino, J.; Janesko, B. G.; Gomperts, R.; Mennucci, B.; Hratchian, H. P.; Ortiz, J. V.; Izmaylov, A. F.; Sonnenberg, J. L.; Williams-Young, D.; Ding, F.; Lipparini, F.; Egidi, F.; Goings, J.; Peng, B.; Petrone, A.; Henderson, T.; Ranasinghe, D.; Zakrzewski, V. G.; Gao, J.; Rega, N.; Zheng, G.; Liang, W.; Hada, M.; Ehara, M.; Toyota, K.; Fukuda, R.; Hasegawa, J.; Ishida, M.; Nakajima, T.; Honda, Y.; Kitao, O.; Nakai, H.; Vreven, T.; Throssell, K.; Montgomery, J. A., Jr.; Peralta, J. E.; Ogliaro, F.; Bearpark, M. J.; Heyd, J. J.; Brothers, E. N.; Kudin, K. N.; Staroverov, V. N.; Keith, T. A.; Kobayashi, R.; Normand, J.; Raghavachari, K.; Rendell, A. P.; Burant, J. C.; Iyengar, S. S.; Tomasi, J.; Cossi, M.; Millam, J. M.; Klene, M.; Adamo, C.; Cammi, R.; Ochterski, J. W.; Martin, R. L.; Morokuma, K.; Farkas, O.; Foresman, J. B.; Fox, D. J., 2016, **Gaussian 16, Revision C.01; Gaussian, Inc., Wallingford CT**.
2. R. D. Senanayake, D. B. Lingerfelt, G. U. Kuda-Singappulige, X. Li and C. M. Aikens, *J. Phys. Chem. C*, 2019, **123**, 14734-14745.
3. R. K. Dennington, T. A.; Millam, J., M., 2016, **GaussView, Version 6; Semichem Inc., Shawnee Mission, KS.**
4. Dana, K.; Shende, C.; Huang, H.; Farquharson, S., *Journal of Analytical & Bioanalytical Techniques* **2015,** *6* (6), 1000289/1-1000289/5.
5. Inscore, F.; Shende, C.; Sengupta, A.; Huang, H.; Farquharson, S., *Applied Spectroscopy* **2011,** *65* (9), 1004-1008.
6. Haddad, A.; Comanescu, M. A.; Green, O.; Kubic, T. A.; Lombardi, J. R., *Anal. Chem.* **2018,** *90* (21), 12678-12685
7. Segawa, H.; Fukuoka, T.; Itoh, T.; Imai, Y.; Iwata, Y. T.; Yamamuro, T.; Kuwayama, K.; Tsujikawa, K.; Kanamori, T.; Inoue, H., *Analyst* **2019,** *144* (23), 6928-6935
8. Raveendran, J.; Dies, H.; Mohammadi, A.; Escobedo, C.; Docoslis, A., *Materials Today: Proceedings* **2018,** *5* (14_Part_1), 27377-27386
9. Yu, W. W.; White, I. M., *Analyst* **2013,** *138* (4), 1020-1025.

10. Deriu, C.; Conticello, I.; Mebel, A. M.; McCord, B., *Analytical Chemistry* **2019,** *91* (7), 4780-4789.
11. N. D. Kline, A. Tripathi, R. Mirsafavi, I. Pardoe, M. Moskovits, C. Meinhart, J. A. Guicheteau, S. D. Christesen and A. W. Fountain, *Anal. Chem.*, **2016**, **88**, 10513-10522.
12. L. Wang, C. Deriu, W. Wu, A. M. Mebel and B. McCord, *J. Raman Spectrosc.*, **2019**, **50**, 1405-1415.